Available online at www.sciencedirect.com
ScienceDirect
Journal of the European Ceramic Society 27 (2007) 2521–2527
www.elsevier.com/locate/jeurceramsoc

Effect of liquid-phase content on the contact-mechanical properties of liquid-phase-sintered α-SiC

Oscar Borrero-López [a], Angel L. Ortiz [a], Fernando Guiberteau [a,*], Nitin P. Padture [b]

[a] *Departamento de Electrónica e Ingeniería Electromecánica, Escuela de Ingenierías Industriales, Universidad de Extremadura, 06071 Badajoz, Spain*
[b] *Department of Materials Science and Engineering, The Ohio State University, Columbus, OH 43210, USA*

Received 24 June 2006; accepted 16 September 2006
Available online 16 November 2006

Abstract

Effect of the content of the intergranular phase ($Y_3Al_5O_{12}$ or yttrium aluminum garnet or YAG) on the room-temperature contact-mechanical properties of pressureless, liquid-phase-sintered (LPS) α-SiC ceramics has been studied. An increase in YAG vol.% is found to result in the expected degradation of the elastic modulus and the indentation yield strength in LPS SiC. However, with increasing YAG vol.% the degradation in the hardness and the sliding-wear resistance is found to be severe, while the indentation toughness first increases and then decreases. These results are analyzed, and discussed in the context of providing guidelines for the design and fabrication of low-cost LPS SiC ceramics with tailored contact-mechanical properties.

Keywords: Liquid-phase sintering; SiC; Mechanical properties

1. Introduction

Pressureless, liquid-phase-sintered (LPS) silicon carbide (SiC) ceramics with oxide additives (Al_2O_3, Y_2O_3) possess remarkable mechanical and thermal properties which, combined with the ease and economy of pressureless processing, makes LPS SiC ceramics attractive structural materials.[1–12]

The mechanical properties of LPS SiC ceramics, at both ambient and elevated temperatures, have been studied extensively.[5–12] However, most of the studies on the mechanical properties of LPS SiC lack a common experimental platform, which precludes the extraction of guidelines for the design of materials with tailored mechanical properties. Therefore, systematic studies aimed at elucidating the roles of the various processing variables on the mechanical properties of LPS SiC are still required. This approach is likely to allow the emulation in LPS SiC of the success achieved over the past decades in the development of silicon nitride (Si_3N_4) structural ceramics—one of the most important advances of the 20th century in engineering ceramics. Moreover, SiC has some advantages over Si_3N_4, such as greater hardness and elastic modulus, superior oxidation resistance, higher thermal conductivity, and lower cost.

Previous studies on LPS SiC have focused on investigating effects of microstructural variables such as grain size, grain aspect ratio, nature and content of the intergranular phase, and SiC polytype composition.[8,9,13–15] In this study we focus on investigating the effect of intergranular phase (YAG) content on the room-temperature contact-mechanical properties of pressureless, LPS α-SiC ceramics. Here we show that YAG vol.% has a profound effect on the hardness, toughness, and sliding-wear resistance of LPS SiC.

2. Experimental procedure

2.1. Processing

The processing procedure used here is identical to the one employed in the earlier studies.[5,16,17] Briefly, six powder batches were individually prepared, each containing α-SiC powder (UF-15, H.C. Stark, Germany), plus a combination of Al_2O_3 (AKP-30, Sumitomo Chemical Company, New York, NY) and Y_2O_3 (Fine Grade, H.C. Starck Inc., Newton, MA) powders in the molar ratio Y_2O_3:Al_2O_3::3:5 to result in YAG liquid-phase during the sintering of SiC. The compositions of the six powder

* Corresponding author.
E-mail address: guiberto@unex.es (F. Guiberteau).

0955-2219/$ – see front matter © 2006 Elsevier Ltd. All rights reserved.
doi:10.1016/j.jeurceramsoc.2006.09.012

batches were designed to yield 3.6 vol.%, 7.3 vol.%, 11.1 vol.%, 15.0 vol.%, 19.1 vol.% or 23.2 vol.% YAG in the sintered materials (abbreviated hereafter as SiC-*x*YAG, where *x* refers to YAG content in vol.%). From each of the powder batches several pellets were uniaxially pressed (Model C, Carver Inc., Wabash, IN) in a steel die (25 mm diameter) at 50 MPa pressure. All pellets were subsequently cold-isostatically pressed (CP360, AIP, Columbus, OH) at a pressure of 350 MPa. Individual pellets were embedded in powder beds inside graphite crucibles with screwable lids. The pellets were sintered in a graphite furnace (Model 1000-3560-FP20, Thermal Technology Inc., Santa Rosa, CA) at 1950 °C for 2 h in flowing Ar-gas atmosphere. The sintered pellets were cleaned and lightly ground to remove any surface reaction layers and/or adhered packing powder.

2.2. Microstructural characterization

Densities of the sintered materials were measured using the Archimedes method, with distilled water as the immersion medium. The relative % densities were calculated using density values of 3.213 g cm^{-3} and 4.544 g cm^{-3} for SiC and YAG, respectively.

Polished cross-sections of the specimens were plasma-etched (PT 1750, Fissions Instruments, East Sussex, UK) for 100–120 min using CF_4 + 4% O_2 gas (300 Pa, 80 W) to reveal the grain boundaries, and were then observed under the scanning electron microscope, SEM (S-3600N, Hitachi, Japan). Several micrographs of representative regions within the microstructures were recorded for grain size analysis. The image analysis procedure described in an earlier study[18] was employed to estimate the longest chord which is defined as the length (*l*), the longest dimension perpendicular to the longest chord is the width (*d*), and the aspect ratio is defined as *l*/*d*. For each sintered material at least 300 grains were used for the grain size analysis.

2.3. Mechanical properties characterization

2.3.1. Hertz indentation

Hertzian indentation tests were performed on each material in a universal testing machine (5535, Instron, Canton, MA) at a constant crosshead speed of 5 μm min^{-1} over a load (*P*) range of 15–4000 N using tungsten carbide spheres of radius (*r*) 1.58–7.94 mm. All the tests were performed at room-temperature in air, following the standard procedure described elsewhere.[19] Briefly, for prescribed values of *P* and *r*, contact radii (*a*) were measured from residual impressions left on the previously polished and gold-coated surfaces, and then used to calculate indentation stress (P_0) and indentation strain (*a*/*r*). These measurements enabled indentation stress-indentation strain curves to be constructed. Based on these curves, the elastic modulus (*E*) was subsequently determined using a standard formula. The indentation yield strength (P_Y) was also estimated from the pressure at which the experimental indentation curve deviates from linearity. For selected materials, P_Y was estimated from direct observation of the minimum indentation pressure required to leave a detectable indentation impression on an uncoated specimen surface.

2.3.2. Vickers indentation

Cross-sections of the sintered materials were ground and polished to a 1-μm finish using routine ceramographic methods. Vickers-indentation tests were performed on the polished specimens to evaluate their hardness (H_V) and toughness (K_{IC}). All Vickers-indentation tests were performed at room-temperature in air using a hardness tester (MV-1, Matsuzawa, Tokyo, Japan), with maximum load (*P*) of 98 N, indentation load rate of 40 μm s^{-1} and dwell time of 20 s. Ten separate indentations were performed for each material. Subsequently, the tested surface was gold-coated for observation under an optical microscope (Epiphot 300, Nikon, Japan). The length of the diagonal of the residual impression and the total length of the surface trace of the radial cracks were then measured under the microscope. The hardness and the toughness were determined using standard formulae.[20,21]

2.3.3. Nanoindentaion tests

Nanoindentations (diamond Berkovich pyramid) were performed on the ceramic with 23.2 vol.% YAG at different surface locations to measure the hardness of the constituents in these two-phase materials, using a Nanoindenter XP (MTS/Nanoinstrument, Oak Ridge, TN) in Dynamic Contact Module^{TM} (DCM) mode. The maximum penetration depth and the penetration speed used were 300 nm and 10 nm/s, respectively. Hardness was evaluated from the indentation load–displacement curves, using standard formulae.[22]

2.3.4. Wear

Several polished disks (7 mm diameter, 2 mm thickness) were core-drilled from the sintered materials for wear testing. Wear testing was performed at room-temperature in a Falex multi-specimen tribometer (Faville-Le Vally Corp., Sugar Grove, IL) using the ball-on-three-disks geometry. Here, a commercial, bearing grade Si_3N_4 ball (NBD 200, Cerbec, East Granby, CT) of radius 6.35 mm rotated in contact with three disk specimens aligned with their surface normals in tetrahedral coordination relative to the rotation axis.[23] Paraffin oil (Heavy Grade, Fisher Scientific, Fair Lawn, NJ) was used as the lubricant (viscosity of ∼3.4 × 10^{-5} m^2 s^{-1} at 40 °C). The contact load on each disk was 70 N and the rotation speed was 100 rpm, corresponding to a sliding velocity of ∼0.04 m s^{-1}. The wear tests were interrupted at intervals, and the diameters of the circular wear scars on each disk were measured using the optical microscope (two orthogonal measurements per disk, three disks per ceramic). The wear-scar diameter was used as quantification of the extent of wear damage. At the end of the wear test (500 min), the wear damage was also observed under the SEM.

3. Results and discussion

Fig. 1A–F are SEM micrographs showing the microstructures of the ceramics considered in this study. The SiC grains and the intergranular YAG are clearly delineated by plasma-etching in the SEM micrographs. The contrast within the SiC grains represents the core-shell structure that develops during liquid-phase sintering, as revealed by plasma etching. The

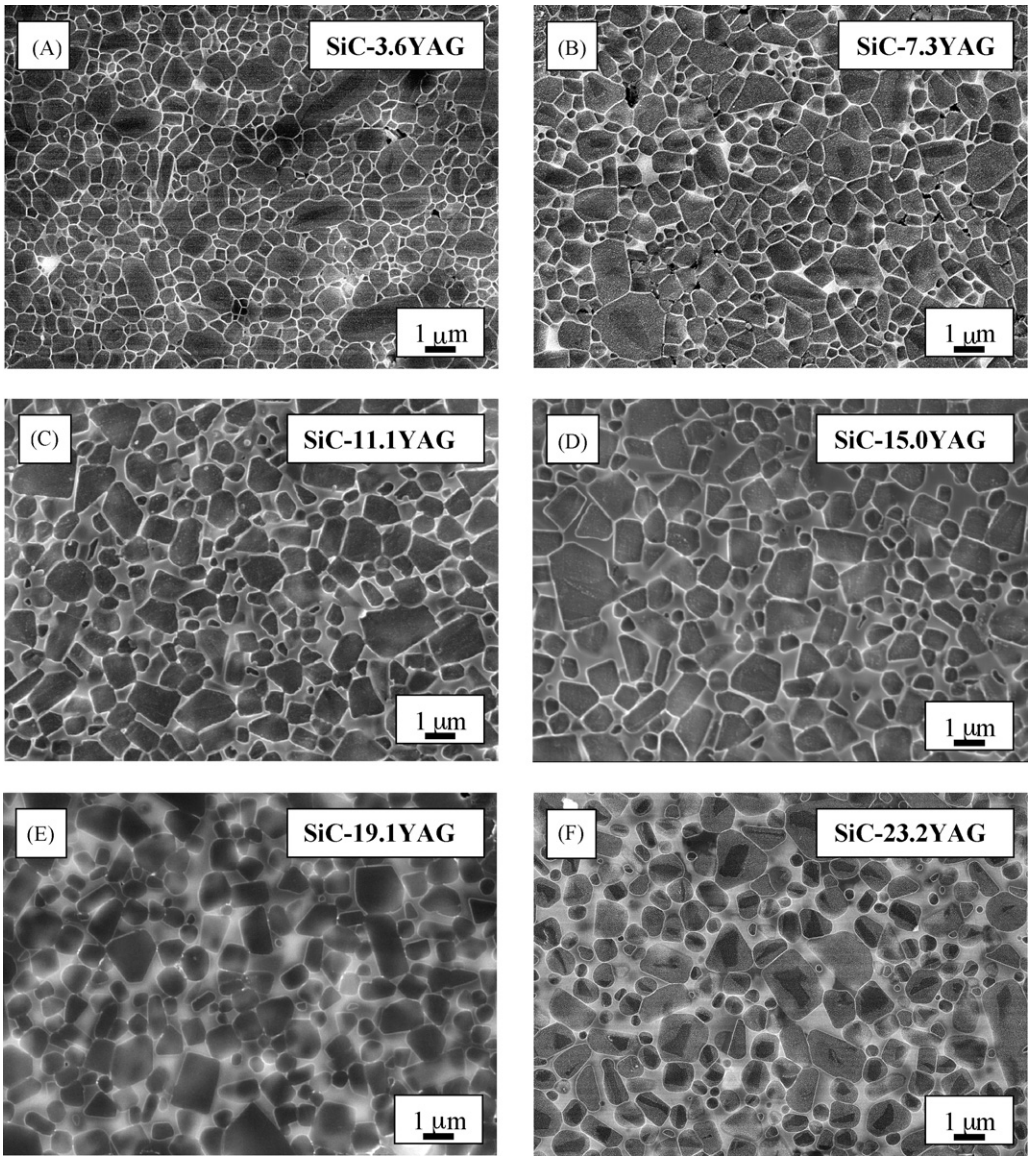

Fig. 1. SEM micrographs of polished and plasma-etched cross-sections of the six LPS SiC ceramics prepared in this study. The light region is crystalline YAG and the darker regions are α-SiC grains. Fig. 1(A), (B) and (F) taken from ref [35].

presence of the core-shell structure indicates that grain growth took place by solution-precipitation (Ostwald ripening).[18,24] The absence of residual porosity in the SEM images indicates that the six ceramics are fully dense, which is consistent with the density values measured by the Archimedes method. It is worth mentioning that fully dense LPS SiC can be obtained using additive amounts as low as 5 wt.%, which is similar to the amount of additives used in solid-state sintering.[25]

Grain size and grain aspect ratio (0.8 μm and 1.4, respectively) are both independent of YAG vol.%, confirming interface-reaction controlled coarsening.[16] The 1.4 aspect ratio corresponds to that of α-SiC grains in equilibrium with a YAG liquid-phase, as demonstrated in an earlier study.[18]

The use of both blunt (Hertz) and sharp (Vickers and Berkovich) indentation techniques allows studies of the mechanical response of the materials from the elastic regime to the plastic regime.[20] Fig. 2 shows the indentation stress–strain plots obtained from Hertzian tests. All six materials show initial linear response at low contact pressures that corresponds to the elastic regime. The elastic moduli of the LPS SiC ceramics calculated from their slope in this regime decrease linearly with increasing YAG vol.% (Fig. 3). This is in close agreement with the rule-of-mixture-model predictions (dashed and dotted lines in Fig. 3), using $E_{SiC} \approx 410$ GPa[26] and $E_{YAG} \approx 282$ GPa.[27] At higher contact pressures, the indentation stress–strain response deviates from linear-elastic response, which is attributed to quasi-plasticity—shear-faulting along weak SiC/YAG interfaces.[2,6] The interface weakness arises from residual stresses induced by the thermal expansion mismatch between SiC and YAG ($\Delta\alpha \sim 5 \times 10^{-6}\,^{\circ}C^{-1}$). These stresses increase with increasing YAG vol.%.[28] This results in the observed decrease in the indentation yield strength (P_Y) — the onset of non-linearity in the indentation stress–strain curves in Fig. 2 — with increasing YAG vol.% (Fig. 4). Note that the P_Y values estimated from

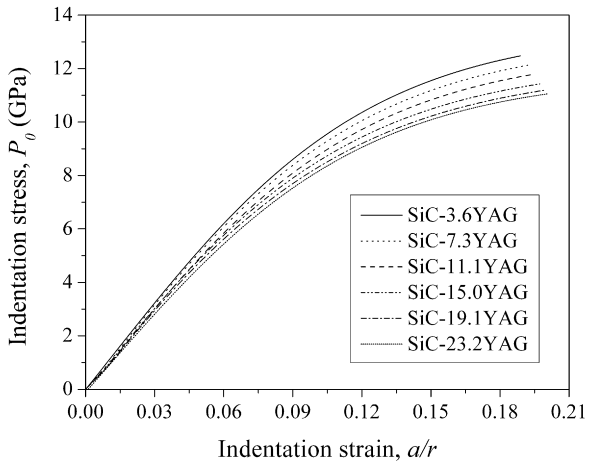

Fig. 2. Indentation stress–strain curves for the six LPS SiC ceramics prepared in this study. The solid lines are the best empirical fits through the experimental data, which are omitted for the sake of clarity.

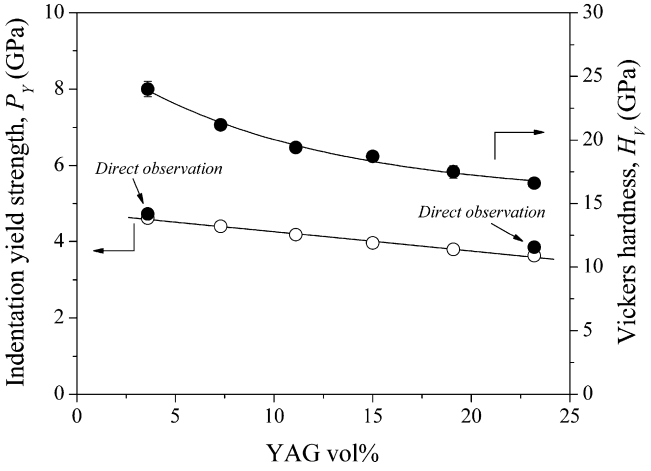

Fig. 4. Indentation yield strength determined by Hertz indentation, and hardness measured by Vickers indentation for the LPS SiC ceramics as a function of YAG vol.%. The solid lines are guides to the eye.

the indentation stress–strain curves are in close agreement with those obtained directly from the minimum indentation pressure required to leave a detectable permanent indentation impression in the SiC-3.6YAG and SiC-23.2YAG materials (Fig. 4).

In Fig. 4, the hardness (H_V) is found to decrease with increasing YAG vol.%. Unlike the linear dependence of P_Y with YAG vol.%, the dependence of H_V with YAG vol.% is exponential-like. The hardness values of pure YAG and pure SiC are 15 and 25 GPa, as determined by nanoindentation of the individual YAG and SiC phases in the SiC-23.2YAG ceramic. For a low YAG content (3.6 vol.%), the plastic deformation of the softer YAG phase is negligible, resulting in a high hardness value, quite similar to that of solid-state-sintered SiC.[29] However, as the YAG vol.% increases, the microstructure of the ceramic is such that the SiC grains are embedded in a continuous YAG matrix. In such microstructures the hardness deformation of the composite is governed by the deformation of the much softer intergranular phase.[30,31] This is why LPS SiC ceramics with YAG content over 15 vol.% have hardnesses that approach the hardness of pure YAG. These results show clearly the detrimental effect of high YAG content on the hardness of LPS SiC.

The fracture toughness of LPS SiC ceramics is found to increase with increasing YAG vol.%, reaching a maximum for 15 vol.% YAG, and then decreases (Fig. 5). The indentation fracture toughness for the LPS SiC with low YAG content (3.6 vol.%) is comparable to that of solid-state-sintered SiC.[32] Fig. 6 shows characteristic crack-propagation patterns in the LPS SiC ceramics with 3.6 vol.%, 15.0 vol.% (corresponding to toughness maximum in Fig. 5), and 23.2 vol.% YAG. It can bee seen that, regardless of the YAG content, fracture is primarily intergranular due to the existence of weak SiC/YAG interfaces,[5] although some transgranular fracture is observed in LPS SiC with YAG content below 15.0 vol.% (arrows in Fig. 6A). Qualitatively, the extent of crack deflection appears to be most effective in SiC-15.0YAG (Fig. 6B), which is perhaps why that ceramic has the highest indentation fracture toughness.

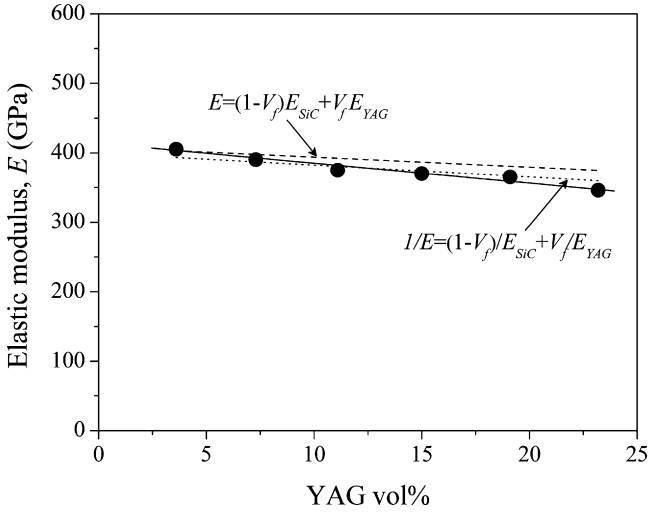

Fig. 3. Elastic modulus for the LPS SiC ceramics as a function of YAG vol.% (V_f). The dashed and dotted lines represent the rule-of-mixtures predictions.

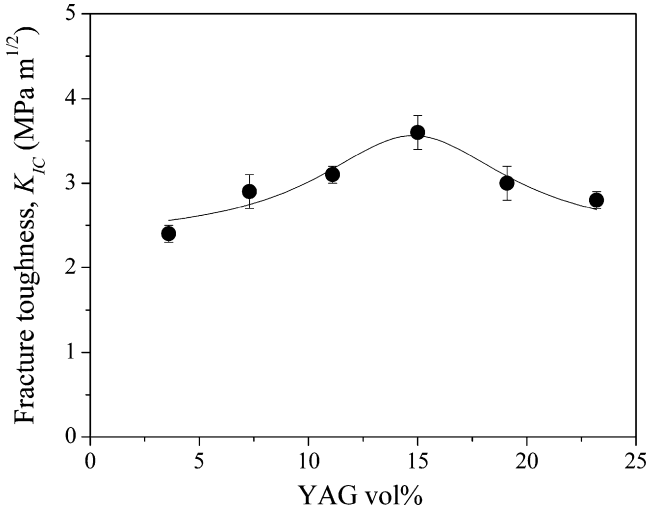

Fig. 5. Fracture toughness values determined from Vickers indentation tests of the LPS SiC ceramics as a function of YAG vol.%. The solid line is a guide to the eye.

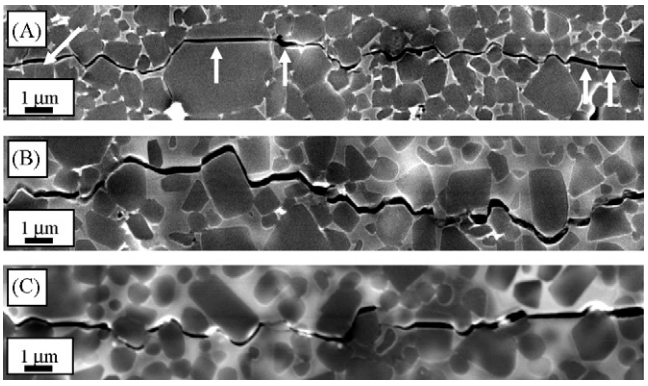

Fig. 6. Characteristic crack-propagation SEM micrographs for selected LPS SiC ceramics containing: (A) 3.6 vol.%, (B) 15.0 vol.% (toughness maximum), and (C) 23.2 vol.% YAG. The observations were conducted near the crack tip.

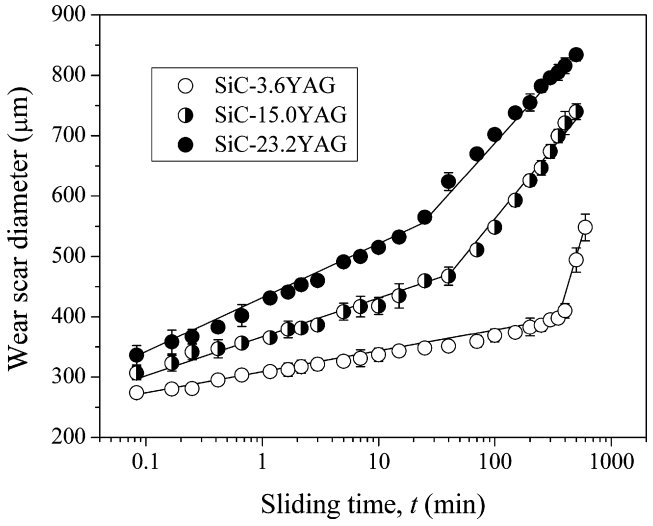

Fig. 7. Wear scar diameter as a function of the sliding time for selected LPS SiC ceramics containing 3.6, 15.0 and 23.2 vol.% YAG. Each datum point represents an average of three specimens tested; error bars represent data range. The solid lines are fits to the data, with the discontinuities in the lines indicating wear transitions. Data for SiC-3.6YAG and SiC-23.2YAG taken from ref [35].

Fig. 7 shows the sliding-wear results for the LPS SiC ceramics with 3.6 vol.%, 15.0 vol.% (corresponding to toughness maximum in Fig. 5), and 23.2 vol.% YAG. All three materials exhibit the two-stage wear-accumulation behavior that has been observed in other polycrystalline ceramics[23,33–37]: mild deformation-controlled wear, followed by severe fracture-controlled wear, with a wear transition. SiC-3.6YAG was found to have the lowest slope in the mild-wear regime, the longest transition time, and the highest slope in the severe-wear regime. The increase in the YAG content led to an increase in both the mild-wear rate and the transition time, and to a decrease in the severe-wear rate (Table 1). These results demonstrate the dramatic effect of the YAG vol.% on the sliding wear of LPS SiC, with SiC-3.6YAG representing the most wear-resistant LPS SiC ceramic obtained in this study. A simple model due to Cho et al.[33] provides a framework for analyzing the sliding-wear results. According to this model, during deformation-controlled wear, plastic-deformation damage (mainly dislocation pile-ups[33,37]) accumulates within the grains as a function of sliding time t, inducing tensile stresses (σ_D) that bear up against the grain boundaries. In addition, tensile thermal stresses from the thermal expansion mismatch (q) are also present. The model then considers "penny"-shaped grain-boundary facet cracks of length βl under the wear contact, where l is the grain size and β is ≤ 1. Those short cracks are subjected to q and $\sigma_D(t)$, resulting a in time-dependent stress intensity factor for such cracks[33]:

$$K(t) = \left(\frac{2}{\pi^{0.5}}\right)(\sigma_D(t) + q)\beta l^{0.5} \quad (1)$$

Despite the various assumptions and simplifications, this model captures the trends in the wear properties of the LPS SiC ceramics: with increasing YAG content, the hardness (H_V) decreases (Fig. 4), and the internal tensile residual stress (q) increases (Table 1). The decreasing hardness results in higher rates at which the dislocation-plasticity induced stress accumulates, and hence higher pre-transition wear rates (m_{pre}); the increasing tensile residual stress (q) will contribute to decreasing the wear-transition time (t_c). This is consistent with the observations (Fig. 7 and Table 1). Therefore, the guidelines for the processing of wear-resistant LPS SiC ceramics — reduction in the intergranular phase content — agree with those for the processing of hard materials.

From Eq. (1), grain-boundary fracture occurs when $K(t)$ reaches ${}^{GB}K_{IC}$, the grain-boundary toughness, at the transition sliding-time $t = t_c$, representing the onset of a transition from deformation- to fracture-controlled wear and subsequent grain pullout. This is confirmed in Fig. 8, showing typical post-transition wear damage in the three ceramics after 500 min sliding. The grooves within the wear scars observed in the optical micrographs suggest that fracture at the microstructural level has taken place. Indeed, grain-boundary fracture and grain pull-out are evident in the SEM micrographs. Also evident is the increase of the wear damage with increasing YAG content, which can also be observed in the optical micrographs. The hard wear particles released after the transition remain under the contact, acting as abrasive particles in further sliding.

Table 1
Sliding-wear properties and associated parameters for selected LPS α-SiC ceramics

Ceramic	Pre-transition slope m (μm)	Wear-transition time t_c (min)	Post-transition slope m (μm)	Effective tensile residual stress, q (MPa)
SiC-3.6YAG	30	350	769	53
SiC-15.0YAG	65	40	230	177
SiC-23.2YAG	90	25	198	231

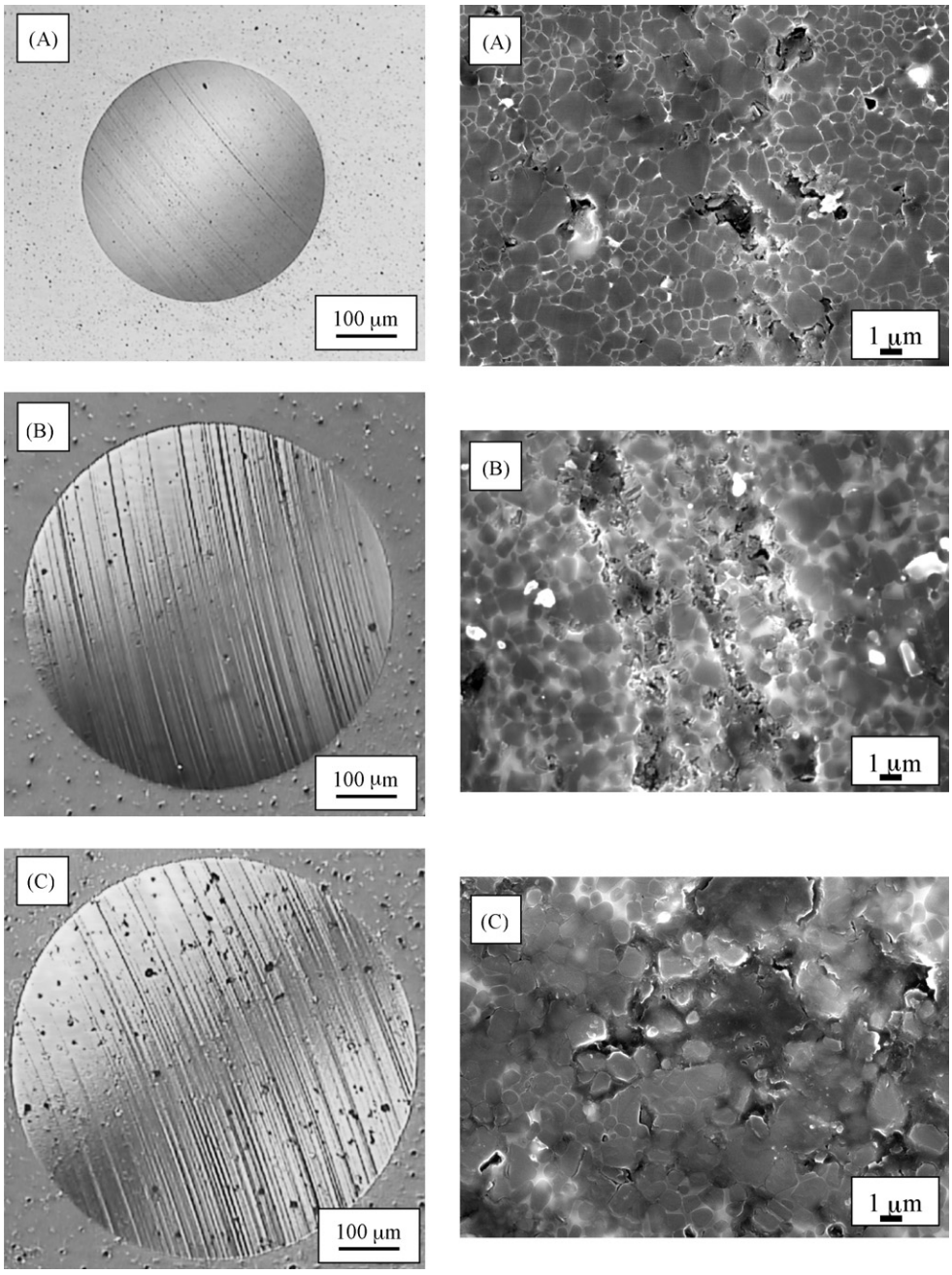

Fig. 8. Optical and SEM micrographs of the wear damage after 500 min of sliding in the ceramics: (A) SiC-3.6YAG, (B) SiC-15.0YAG, and (C) SiC-23.2YAG. The presence of grooves in the optical images is indicative of the fracture-controlled wear regime, which is also evident from severe grain-boundary fracture and grain pull-out in the SEM images. Fig.8(C) taken from ref [35].

4. Conclusions

We have studied the effect of the content of the intergranular YAG phase on the microstructure and the room-temperature contact-mechanical properties of LPS α-SiC ceramics, for extracting key guidelines for the design and processing of low-cost SiC-based ceramics with tailored mechanical properties. Based on these studies the following conclusions can be drawn:

- The grain size and grain aspect ratio in LPS SiC ceramics are both independent of the intergranular phase content, revealing that grain-growth kinetics are interface-reaction controlled.
- The elastic modulus, the indentation yield strength, and the hardness decrease with increasing YAG content.
- The fracture mode in LPS SiC is primarily intergranular. With the increase in the YAG content, the indentation fracture toughness first increases due to enhanced crack-bridging toughening, and then decreases.
- The sliding-wear of LPS SiC exhibits two successive regimes: (i) plastic deformation-controlled wear, followed by an abrupt transition to (ii) fracture-controlled wear, with a much higher

wear rate due to severe grain-boundary fracture and grain pull-out. The increase in YAG content leads to degradation in the sliding-wear resistance.

Acknowledgements

This work was supported by the Ministerio de Ciencia y Tecnología (Government of Spain), and the Fondo Europeo de Desarrollo Regional (FEDER), under grants Nos. CICYT MAT 2004-05971 and UNEX00-23-013

References

1. Suzuki, K. and Sasaki, M., Pressureless sintering of silicon carbide. In *Fundamental structural ceramics*, ed. S. Somiya and R. C. Bradt. Terra Scientific Publishing Company, Tokyo, Japan, 1987, pp. 75–87.
2. Lawn, B. R., Padture, N. P., Cai, H. and Guiberteau, F., Making ceramics 'ductile'. *Science*, 1994, **263**(5150), 1114–1116.
3. Sigl, L. S., Thermal conductivity of liquid phase sintered silicon carbide. *J. Eur. Ceram. Soc.*, 2003, **23**(7), 1115–1122.
4. Zhou, Y., Hirao, K., Yamaguchi, Y. and Kanzaki, S., Effects of rare-earth oxide and alumina additives on thermal conductivity of liquid-phase-sintered silicon carbide. *J. Mater. Res.*, 2003, **18**(8), 1854–1862.
5. Padture, N. P., *In situ*-toughened silicon carbide. *J. Am. Ceram. Soc.*, 1994, **77**(2), 519–523.
6. Padture, N. P. and Lawn, B. R., Toughness properties of a silicon carbide with *in situ*-induced heterogeneous grain structure. *J. Am. Ceram. Soc.*, 1994, **77**(10), 2518–2522.
7. Lee, S. K., Kim, D. K. and Kim, C. K., Flaw-tolerance and *R*-curve behavior of liquid-phase-sintered silicon carbides with different microstructures. *J. Am. Ceram. Soc.*, 1995, **78**(1), 65–70.
8. Baud, S. and Thevenot, F., Microstructures and mechanical properties of liquid-phase sintered seeded silicon carbide. *Mater. Chem. Phys.*, 2001, **67**(1-3), 165–174.
9. Ortiz, A. L., Muñoz-Bernabé, A., Borrero-López, O., Domínguez-Rodríguez, A., Guiberteau, F. and Padture, N. P., Effect of sintering atmosphere on the mechanical properties of liquid-phase-sintered SiC. *J. Eur. Ceram. Soc.*, 2004, **24**(10–11), 3245–3249.
10. Borrero-López, O., Ortiz, A. L., Guiberteau, F. and Padture, N. P., Room-temperature mechanical properties of liquid-phase-sintered alpha-SiC with Y_2O_3-Al_2O_3 additions. *Bol. Soc. Esp. Ceram. V.*, 2005, **44**(5), 265–269.
11. Castillo-Rodríguez, M., Muñoz, A. and Domínguez-Rodríguez, A., Effect of atmosphere and sintering time on the microstructure and mechanical properties at high temperatures of α-SiC sintered with liquid phase Y_2O_3–Al_2O_3. *J. Eur. Ceram. Soc.*, in press.
12. Jensen, R. P., Luecke, W. E., Padture, N. P. and Wiederhorn, S. M., High-temperature properties of liquid-phase-sintered alpha-SiC. *Mater. Sci. Eng. A*, 2000, **282**(1-2), 109–114.
13. Kim, Y.-W., Mitomo, M., Emoto, H. and Lee, J. G., Effect of initial α-phase content on microstructural and mechanical properties of sintered silicon carbide. *J. Am. Ceram. Soc.*, 1998, **81**(12), 3136–3140.
14. Nader, M., Aldinger, F. and Hoffmann, M. J., Influence of the α/β-SiC phase transformation on microstructural development and mechanical properties of liquid phase sintered silicon carbide. *J. Mater. Sci.*, 1999, **34**(6), 1197–1204.
15. Sciti, D., Guicciardi, S. and Bellosi, A., Effect of annealing treatments on microstructure and mechanical properties of liquid-phase-sintered silicon carbide. *J. Eur. Ceram. Soc.*, 2001, **21**(5), 621–632.
16. Ye, H., Pujar, V. V. and Padture, N. P., Coarsening in liquid-phase-sintered α-SiC. *Acta Mater.*, 1999, **47**(2), 481–487.
17. Pujar, V. V., Jensen, R. P. and Padture, N. P., Densification of liquid-phase-sintered SiC. *J. Mater. Sci. Lett.*, 2000, **19**(11), 1011–1014.
18. Xu, H., Bhatia, T., Deshpande, S. A., Padture, N. P., Ortiz, A. L. and Cumbrera, F. L., Microstructural evolution in liquid-phase-sintered SiC. I. Effect of starting SiC powder. *J. Am. Ceram. Soc.*, 2001, **84**(7), 1578–1584.
19. Guiberteau, F., Padture, N. P. and Lawn, B. R., Effect of grain size on hertzian contact damage in alumina. *J. Am. Ceram. Soc.*, 1994, **77**(7), 1825–1831.
20. Lawn, B. R., *Fracture of brittle solids* (*2nd ed.*). Cambridge University Press, Cambridge, UK, 1993.
21. Anstis, G. R., Chantikul, P., Marshall, D. B. and Lawn, B. R., A critical evaluation of indentation techniques for measuring fracture toughness. I. Direct crack measurements. *J. Am. Ceram. Soc.*, 1981, **64**(9), 533–538.
22. Oliver, W. C. and Pharr, G. M., An improved technique for determining hardness and elastic-modulus using load and displacement sensing indentation experiments. *J. Mater. Res.*, 1992, **7**(6), 1564–1583.
23. Thompson, S. C., Pandit, A., Padture, N. P. and Suresh, S., Stepwise-graded Si_3N_4-SiC ceramics with improved wear properties. *J. Am. Ceram. Soc.*, 2002, **85**(8), 2059–2064.
24. Sigl, L. S. and Kleebe, H.-J., Core/rim structure of liquid-phase-sintered silicon carbide. *J. Am. Ceram. Soc.*, 1993, **76**(3), 773–776.
25. Prochazka, S., Densification of silicon-carbide. *Am. Ceram. Soc. Bull.*, 1974, **53**(4), 319.
26. Richerson, D. W., *Modern ceramic engineering*. Marcel Dekker, New York, 1992.
27. deWith, G. and Parren, J. E. D., Translucent $Y_3Al_5O_{12}$ ceramics: mechanical properties. *Solid State Ionics*, 1985, **16**(1-4), 87–93.
28. Lawn, B. R., Padture, N. P., Braun, L. M. and Bennison, S. J., Model for toughness curves in two-phase ceramics. I. Basic fracture mechanics. *J. Am. Ceram. Soc.*, 1993, **76**(9), 2235–2240.
29. Quinn, J. B. and Quinn, G. D., Indentation brittleness of ceramics: a fresh approach. *J. Mater. Sci.*, 1997, **32**(16), 4331–4346.
30. She, J. H. and Ueno, K., Effect of additive content on liquid-phase sintering on silicon carbide ceramics. *Mater. Res. Bull.*, 1999, **34**(10-11), 1629–1636.
31. Engqvist, H., Jacobson, S. and Axen, N., A model for the hardness of cemented carbides. *Wear*, 2002, **252**(5-6), 384–393.
32. Munro, R. G., Material properties of a sintered α-SiC. *J. Phys. Chem. Ref. Data*, 1997, **26**(5), 1195–1203.
33. Cho, S.-J., Hockey, B. J., Lawn, B. R. and Bennison, S. J., Grain-size and R-curve effects in the abrasive wear of alumina. *J. Am. Ceram. Soc.*, 1989, **72**(7), 1249–1252.
34. Hsu, S. M. and Shen, M., Wear prediction of ceramics. *Wear*, 2004, **256**(9-10), 867–878.
35. Borrero-Lopez, O., Ortiz, A. L., Guiberteau, F. and Padture, N. P., Effect of microstructure on sliding-wear properties of liquid-phase-sintered α-SiC. *J. Am. Ceram. Soc.*, 2005, **88**(8), 2159–2163.
36. Borrero-Lopez, O., Ortiz, A. L., Guiberteau, F. and Padture, N. P., Improved sliding-wear resistance in *In-Situ* toughened silicon carbide. *J. Am. Ceram. Soc.*, 2005, **88**(12), 3531–3534.
37. Cho, S.-J., Um, C.-D. and Kim, S.-S., Wear and wear transition mechanism in silicon carbide ceramics during sliding. *J. Am. Ceram. Soc.*, 1995, **78**(4), 1076–1078.